Orbitally defined field-induced electronic state in a Kondo lattice

G. G. Lesseux,[1] H. Sakai,[2] T. Hattori,[2] Y. Tokunaga,[2] S. Kambe,[2] P. L. Kuhns,[3] A. P. Reyes,[3] J. D. Thompson,[4] P. G. Pagliuso,[1] and R. R. Urbano[1]

[1]*Instituto de Física "Gleb Wataghin", Universidade Estadual de Campinas, 13083-859, Campinas, SP, Brazil*
[2]*Advanced Science Research Center, Japan Atomic Energy Agency, Tokai, Ibaraki, 319-1195, Japan*
[3]*National High Magnetic Field Laboratory, Florida State University, Tallahassee, Florida 32310, USA*
[4]*Los Alamos National Laboratory, Los Alamos, New Mexico 87545, USA*

(Received 12 June 2019; revised manuscript received 12 March 2020; accepted 13 March 2020; published 10 April 2020)

$CeRhIn_5$ is a Kondo-lattice prototype in which a magnetic field $B^* \simeq 31$ T induces an abrupt Fermi-surface (FS) reconstruction and pronounced in-plane electrical transport anisotropy all within its antiferromagnetic state. Though the antiferromagnetic order at zero field is well understood, the origin of an emergent state at B^* remains unknown due to challenges inherent to probing states microscopically at high fields. Here we report low-temperature nuclear magnetic resonance (NMR) measurements revealing a pronounced decrease in the ^{115}In formal Knight shift, without changes in crystal or magnetic structures, of $CeRhIn_5$ at fields ($\|c$) spanning B^*. We discuss the emergent state above B^* in terms of a change in Ce's $4f$ orbitals that arises from field-induced evolution of crystal-electric field (CEF) energy levels. This change in orbital character enhances hybridization between the $4f$ and the conduction electrons that leads ultimately to an itinerant quantum-critical point at $B_{c0} \simeq 50$ T.

DOI: 10.1103/PhysRevB.101.165111

Development of the peculiar electronic state above $B^* \simeq 31$ T in $CeRhIn_5$ is signaled clearly in quantum oscillations [1], magnetoresistance [1,2], magnetostriction [3], but not in specific heat [4]. The lack of a detectable specific heat anomaly suggests that B^* may not reflect a well-defined phase transition but a crossover from one state to another [3] where not only the Fermi surface (FS) reconstructs from small-to-large [1] but also in-plane anisotropy develops in electrical resistivity [5]. Qualitatively, these responses could be consistent with a field-induced change in crystal and or magnetic structure from below to above B^*—a distinctly plausible interpretation that could be tested straightforwardly by a diffraction measurement if B^* were sufficiently low to be accessible in neutron or x-ray experiments. Even if such measurements could be made at fields to 30 T and higher, experiments point to a more complex picture, with similarities to other correlated electron systems. Electrical resistivity studies reveal a hysteretic transition at B^* that was interpreted initially to reflect the formation of a density wave, analogous to that found in correlated copper-oxide materials [2]. More recent studies are even more surprising [5]: when an applied field is tipped about 20° from the tetragonal c axis toward in-plane perpendicular directions, there is a striking inequivalence of electrical resistivity for current flow along each pair of orthogonal crystallographic directions. This unexpected in-plane symmetry breaking is consistent with a proposed strong XY nematic susceptibility that is similar to but distinct from Ising nematicity that is found in high-T_c copper oxide [6,7], iron-pnictide [8,9], and correlated ruthenate materials [10].

Evidence for all the changes in electronic properties at B^* and their weak coupling to the crystal lattice [3,5] appears only within the magnetically ordered state of $CeRhIn_5$. In this limit, partially Kondo-compensated Ce moments order below $T_N = 3.8$ K in a spin-spiral structure with ordering wave-vector $\boldsymbol{Q} = (0.5, 0.5, 0.297)$ and moments in the tetragonal plane [11]. This structure, however, is unstable against modest applied pressure [12] or in-plane applied magnetic field [11,13,14]. The near degeneracy of accessible orders in $CeRhIn_5$ supports the possibility that a field of 30 T could change the nature of magnetism at B^*, but with little change in entropy or susceptibility. What might underlie the emergence of the new electronic state above B^* and a change in magnetic character, if this indeed happens, are fundamental questions raised by recent discoveries in $CeRhIn_5$ and are relevant more broadly to the physics of a Kondo lattice.

With its sensitivity to local spin, charge, and lattice degrees of freedom [16,17], NMR is a powerful tool to probe the evolution of complex electronic states in correlated electron materials at very high magnetic fields [18–21]. Figures 1(b)–1(d) presents the ^{115}In NMR spectra ($I = 9/2$) from two inequivalent sites of our $CeRhIn_5$ single crystal with B applied along the c axis at 0.5 K below $T_N(B)$. As shown in Fig. 1(a), each Ce atom is surrounded by four tetragonally coordinated In(1) and eight In(2) atoms with local orthorhombic symmetry. At low fields [Fig. 1(b)], there are nine equally separated transitions associated with In(1) NMR. In contrast, the lower relative intensities of the In(2) NMR signal are a consequence of spectral broadening due to a distribution of internal fields arising from an oscillating hyperfine (internal) field $B_{\rm int}^{\|c}(2)$ associated with c-axis incommensuration of the spin-spiral magnetic structure [22,23].

At low fields and well below T_N, a hyperfine field of $B_{\rm int}^{\perp c}(1) = 0.17$ T lies in the Ce-In(1) (ab) plane and rotates between the adjacent layers with the incommensurate pitch of

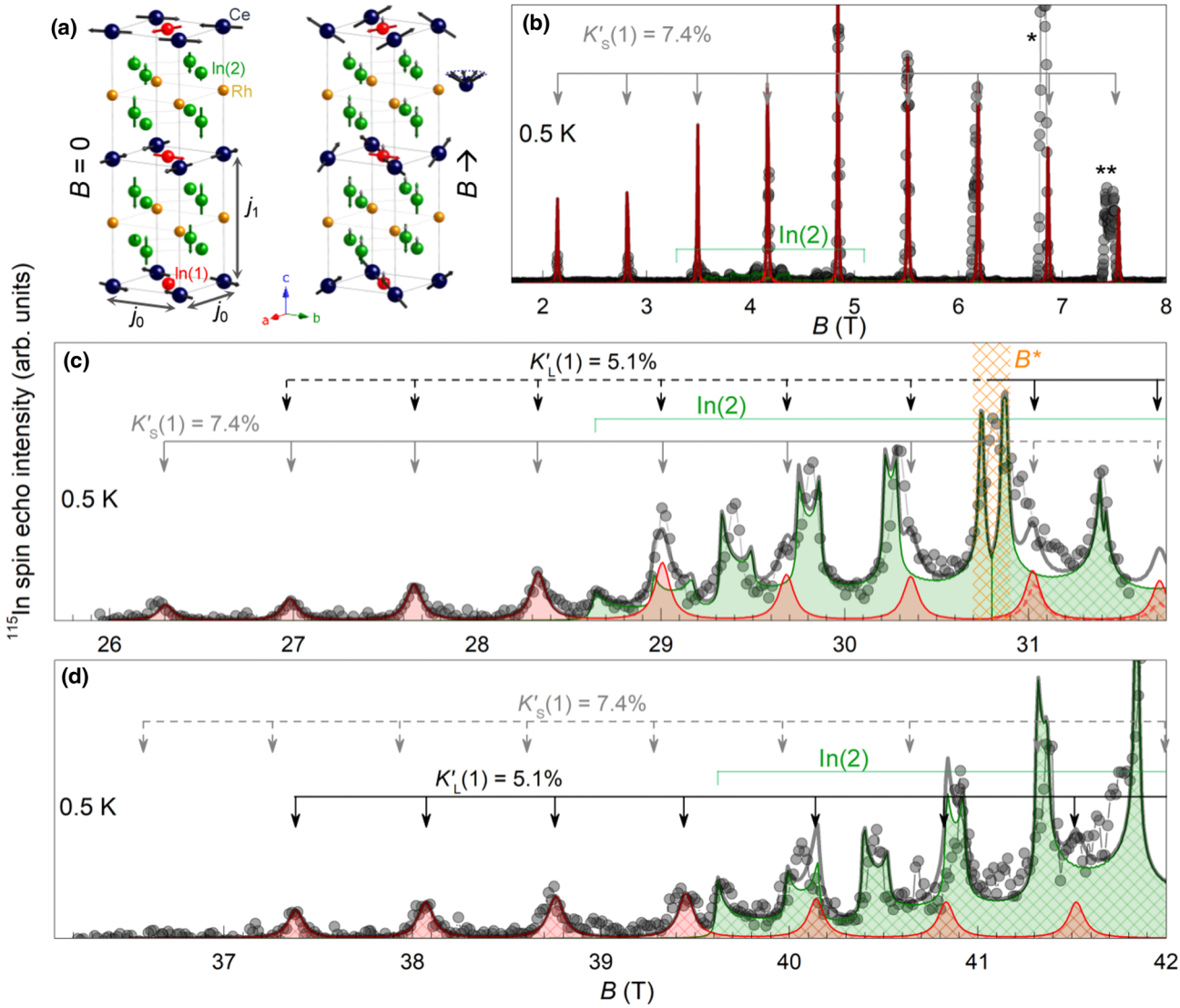

FIG. 1. $CeRhIn_5$ structural properties and ^{115}In NMR spectra with $B\|c$. (a) $CeRhIn_5$ crystallographic structure. The Ce, Rh, In(1), and In(2) sites are indicated in dark blue, yellow, red, and green, respectively. In the left figure we also show the magnetic structure (black arrows at the Ce site) for zero field and, in the right figure, how the magnetic structure evolves to a conical configuration by applying a magnetic field along the c axis. The respective hyperfine (internal) fields for In(1) and In(2) sites are indicated by red and green arrows, respectively. The field-induced hyperfine (internal) field at In(1) and In(2) sites are indicated by gray arrows in the right figure. (b)–(d) NMR spectra of In(1) and In(2) measured at 0.5 K for excitation frequencies 48.5 MHz (b), 290.65 MHz (c), and 393.6 MHz (d). Light gray symbols are data. An Al-NMR signal (not shown) was used as a field marker. The probe used to acquire the 48.5 MHz spectrum shows extrinsic NMR signals, marked with * and **, from ^{207}Pb and/or ^{209}Bi present in the solder and coaxial cable in the NMR circuit visible at 0.5 K, $B \sim 6.8$ T, and 7.5 T. These signals are not present in the high field spectra (c) and (d) obtained with a different probe. The shaded red areas are simulations for the In(1) equidistant transitions, and the green area indicates a simulation for the incommensurate In(2) pattern [15]. The solid gray curve is the overall In-NMR simulated spectrum that includes both contributions. The nonhashed and hashed areas indicate the formal Knight shifts of In(1) and In(2) below $[K'_S(1) = (7.4 \pm 0.1)\%, K'_S(2) = (1.5 \pm 0.2)\%]$ and above $[K'_L(1) = (5.1 \pm 0.1)\%, K'_L(2) = (1.1 \pm 0.2)\%]$ $B^* \sim 30.8$ T. The subscripts S and L for the magnetic phases with a small and large Fermi surfaces. B^* is indicated by a vertical orange dashed strip in (c). The vertical gray and black arrows indicate the expected In(1) transitions for formal Knight shifts $K'_S(1) = 7.4\%$ and $K'_L(1) = 5.1\%$, respectively. The solid and dashed arrows indicate whether In(1) transitions were observed (solid) or not (dashed). Although smaller, there also is a change in $K'(2)$ as well, which follows the same trend as $K'(1)$ and is discussed in the text. The difference between gray and black arrows indicates a change in the shift $\Delta K'(1)$ for fields above $B^* \sim 31$ T, but the line shape and width of the transitions remain similar across B^*. To assure confidence in these high-field measurements we measured a spectrum at 290.65 MHz while sweeping the field up and at 393.6 MHz in a down-field sweep. Results were reproducible.

the magnetic structure shown in Fig. 1(a) [22,23]. At higher fields with B applied along the c axis, $B_{\rm int}^{\perp c}(1)$ can be neglected $[B \gg B_{\rm int}^{\perp c}(1)]$. The magnetic field along the c axis induces a canting of the Ce local moment [13] [Fig. 1(a)] leading to extra internal fields $B_{\rm int}^{\|c}(1)$ and $B_{\rm int}^{\|c}(2)$ at both In(1) and In(2) sites, respectively. Therefore the local effective field at In(1)

can be modeled as

$$B_{\rm local}(1) \simeq [1 + K^{\|c}_{\rm c.e.}(1)]B + B^{\|c}_{\rm int}(1). \quad (1)$$

For the Kondo-lattice $CeRhIn_5$, the first term in Eq. (1) is associated with a contribution from itinerant quasiparticles, therefore proportional to the density of states in the Fermi level, and the second term with the internal field at In(1) due to the out-of-plane Ce-moment component. This internal field component $B^{\|c}_{\rm int}(1) = A^{\|c}_{\rm ord}\mu_{\rm Ce}\cos(\beta/2)$, where $A^{\|c}_{\rm ord}$ is the diagonal c component of the hyperfine coupling tensor from the ordered local moments, $\mu_{\rm Ce}$ is the Ce local moment, and β is the angle of the conical spin structure [see Fig. 1(a)]. Because $B^{\|c}_{\rm int}$ is proportional to B due to the Zeeman interaction, thus the local internal field $B_{\rm local}(1)$ at In(1) sites is

$$B_{\rm local}(1) = [1 + K'(1)]B, \quad (2)$$

with $K'(1)$ defining the formal In(1) Knight shift that bears contributions from both local and itinerant spin susceptibilities. In the case of In(2), the hyperfine field resulting from the in-plane ordered Ce moments follows the oscillatory noncommensurate character of the magnetic structure $B^{\|c}_{\rm int,0}(2) = B_{i0}\cos(2\pi Q_z z)$ [Fig 1(a)]. The out-of-plane contribution of the Ce moments for the hyperfine field at the In(2) site lies in the c direction [24–26] and is also proportional to the external field due to the Zeeman interaction, the local field at an In(2) site can be defined in terms of a formal Knight shift $K'(2)$:

$$B_{\rm local}(2) = [1 + K'(2)]B + B^{\|c}_{\rm int,0}(2). \quad (3)$$

As indicated by solid vertical (gray) arrows in Figs. 1(b) and 1(c), below $B^* \sim 30.8$ T the position of In(1) transitions can be calculated (see the Supplemental Material [15]) assuming a formal Knight shift $K'_{\rm S}(1) = (7.4 \pm 0.1)\%$ and quadrupolar frequency $\nu_Q = 6.77(1)$ MHz. The subscript S denotes the phase below B^* with a small Fermi surface while L stands for the phase above B^*. This formal Knight shift bears contributions from both local and itinerant spin susceptibilities. The value of $K'_{\rm S}(1)$ is consistent with the paramagnetic value [27] of $K^{\|c}_{\rm PM}(1) \simeq 8.0\%$. The spectrum from In(2) in the AFM phase can be calculated similarly by assuming a periodically oscillating internal field $B^{\|c}_{\rm int,0}(2) = 0.27$ T along the c axis [23], with nearly the same low-field quadrupolar parameters [22,28] and a formal Knight shift $K'_{\rm S}(2) = (1.5 \pm 0.1)\%$. Taking these parameters into account, we calculate the ^{115}In NMR spectrum that is given by red and green colors for contributions from In(1) and In(2), respectively. The gray solid curve is the simulated (convoluted) overall ^{115}In NMR spectrum from both In signals.

The simulated spectra in Fig. 1(c) are made on the basis of low-field NMR parameters [22,28] that account well for the spectra in Fig. 1(b) and agree with experiment for fields up to 30.8 T where some deviation from simulation and experimental results begins just where the new AF_L phase sets in. However, above $B^* \simeq 30.8$ T, the spectra are well simulated by keeping all low-field nuclear quadrupolar parameters but with a decrease of both In(1) and In(2) formal shifts from $K'_{\rm S}(1) = (7.4 \pm 0.1)\%$ to $K'_{\rm L}(1) = (5.1 \pm 0.1)\%$ and $K'_{\rm S}(2) = (1.5 \pm 0.1)\%$ to $K'_{\rm L}(2) = (1.1 \pm 0.2)\%$, respectively, indicating the absence of a detectable local structural distortion or a significant change in magnetic structure at B^*.

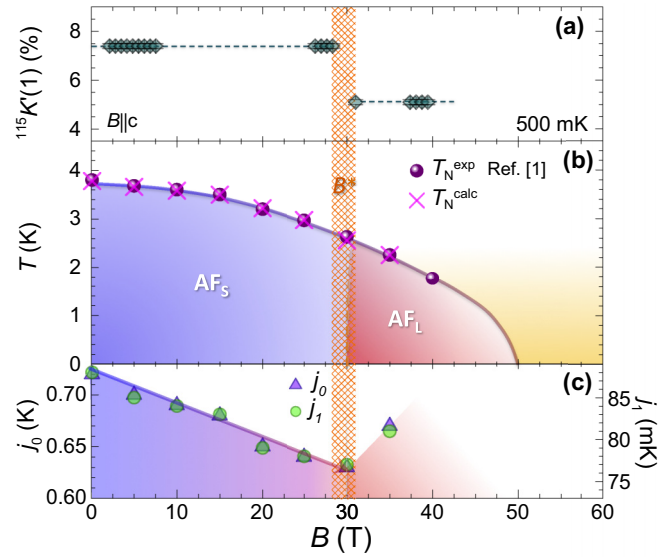

FIG. 2. Formal Knight shift and magnetic properties of $CeRhIn_5$. (a) In(1) formal Knight shift at 0.5 K as a function of magnetic field, with a prominent decrease at B^* where the In(2) formal shift also decreases. See text for details. (b) Field-dependent Néel boundary determined with $B \parallel c$. Solid circles are measured values [1] and crosses are calculated from a mean-field model with CEF, Zeeman, and effective RKKY interactions and, for the set of coupling constants j_0 and j_1 shown in (c). See text for a discussion.

The simulation remains comparably good at fields well above B^* [Fig. 1(d)]. The larger $\Delta K'(1)$ compared to $\Delta K'(2)$ is consistent with the larger hyperfine coupling constant of In(1) [29], but the relative decrease of $K'(1)$ and $K'(2)$ is similar. Figure 2(a) summarizes the field dependence of the In(1) Knight shift. The decrease in formal In(1) and In(2) Knight shifts above B^* implies a decrease in bulk magnetization [30] in the high-field state that is reflected in part by a decrease in the slope of the c-axis magnetization around B^* [13]. Opening a density-wave gap in the reconstructed large Fermi surface is consistent with the decrease in formal shifts if $K_{\rm c.e.}$, which is proportional to the susceptibility of itinerant quasiparticles, dominates $K'_{\rm L}$. This is a scenario proposed previously [1,2], but, as we have concluded, the nesting wave vector that opens a gap must be similar to the zero-field $\boldsymbol{Q}$. A related scenario is that the decrease in formal Knight shifts is due to a decrease in internal field $B^{\|c}_{\rm int}(1)$ that arises from a reduction of the ordered moment $\mu_{\rm Ce}$, and/or a decrease of the hyperfine coupling constant $A^{\|c}_{\rm ord}$. Both of these depend on the extent to which Ce's $4f$ electrons hybridize with band electrons [30] and, in the limit of stronger hybridization, would reflect additional f spectral weight being transferred to band states [31], with a corresponding increase of the FS. Because a magnetic field tends to weaken Kondo hybridization as it polarizes spins of both conduction and localized electrons, this scenario superficially seems unlikely but as discussed below is supported by simplified model calculations.

From the high-field data and spectra simulation, we can conclude that the magnetic structure does not change qualitatively through B^*. One possibility is that the magnetic structure adopts the commensurate order with $\boldsymbol{Q} = (0.5, 0.5, 0.25)$

observed for $CeRhIn_5$ when $B^{\perp c} \gtrsim 2$ T [11,14] that is not so different from the low-field incommensurate $\boldsymbol{Q} = (0.5, 0.5, 0.297)$. For a commensurate $\boldsymbol{Q}$, the internal field $B^{\parallel c}_{\text{int},0}(2)$ at In(2) will take only distinct values, but an incommensurate $\boldsymbol{Q}$ creates an oscillating $B^{\parallel c}_{\text{int},0}(2)$ that produces a characteristic "double horn" spectral distribution pattern. Such a distribution is, indeed, revealed by the NMR data and simulation presented in Figs. 1(c) and 1(d). We conclude that the magnetic structure of $CeRhIn_5$ remains incommensurate with a similar, if not identical, $\boldsymbol{Q} = (0.5, 0.5, 0.297)$ above B^*.

At high fields, the In spectrum, acquired in a hybrid 45 T magnet, broadens as shown in Figs. 1(c) and 1(d). This broadening is more evident for the equidistant In(1) transitions where the linewidth increases from $\Delta L \simeq 0.020(5)$ T in the low-field limit to $\Delta L \simeq 0.10(1)$ T in the high-field limit. We consider possibilities for this broadening. Though not dramatically, the linewidth increases with increasing fields from 26 to 42 T, which likely is due to the crystal experiencing a slight field gradient in the hybrid magnet. From the magnet's known (in)homogeneity, we estimate that the linewidth would increase by at most 9% in this field range. Field-induced electronic anisotropy from the proposed XY nematicity [5] in principle should contribute to NMR line broadening. Such a nematic electronic texture would induce anisotropy in the in-plane hyperfine field component at the In(1) site [Fig. 1(a)], resulting in line broadening or even splitting each In(1) transition, and by breaking local tetragonal symmetry of the In(1) site, would produce nonequidistant In(1) transitions due to a modified electric field gradient (EFG). Within the accuracy of our measurements, however, the separation between In(1) transitions remains constant for fields spanning B^*, and there is no clear evidence for splitting of In(1) transitions. Though the pronounced in-plane symmetry breaking of magnetotransport appears at B^*, weak magnetoresistive anisotropy begins to develop [5] already near 17 T where specific heat and de Haas–van Alphen measurements with field along the c axis also find the onset of enhanced Sommerfeld coefficient and quasiparticle mass [4]. Whether these effects are precursors to proposed nematicity above B^* is unknown but, whatever their origin, conceivably could manifest in larger linewidths shown in Figs. 1(c) and 1(d). Nevertheless, In(1) line shapes remain symmetric and do not broaden noticeably as field is swept through B^*. The absence of a change in crystal and magnetic structures as a function of field and particularly the decrease in formal Knight shift at B^* [Fig. 2(a)] are primary conclusions that come directly from our NMR measurements. In particular, the absence of change in the magnetic structure means that the later remains incommensurate along the c axis with a propagation wave vector $\boldsymbol{Q} = (0.5, 0.5, Q_z)$ at fields spanning B^*.

The ground states of $CeRhIn_5$ and its isostructural family members $CeCoIn_5$ and $CeIrIn_5$, depend on the orbital character of their $4f$ wave functions that determines the extent of f hybridization with In electronic states [32]. In a tetragonal environment, the CEF splits the $J = 5/2$ manifold of $CeRhIn_5$'s $4f^1$ state into three doublets whose energy separation and wave functions (see the Supplemental Material [15]) have been determined by linear-polarized soft-x-ray absorption and inelastic neutron scattering experiments in zero magnetic field [33,34]. Fields of order $B^* \simeq 30$ T ($\Delta_{\text{CEF}} \simeq 7$ meV $\simeq 81$ K) are sufficient to induce mixing of the wave functions of the Γ^2_7 doublet ground state with the first excited doublet state Γ^1_7. This level mixing manifests as a bending of the field-dependent CEF energy levels and slope change in the field-dependent magnetization (see the Supplemental Material [15] and also Refs. [33–35] therein).

We now consider the consequences of magnetic degrees of freedom. Although a general solution of a theory of a strongly interacting Kondo lattice like $CeRhIn_5$ has not been solved, we incorporate the magnetic Rudderman-Kittel-Kasuya-Yosida (RKKY) interaction into the above electronic framework. This magnetic interaction is represented by an effective spin-spin interaction term $j_k \mathbf{J_m} \cdot \mathbf{J_n}$. Specifically, we consider a simplified mean-field model with intra- and interlayer nearest-neighbor (n.n.) exchange couplings [$j_x = j_y \equiv j_0$ and $j_z \equiv j_1$, Fig. 1(a)] to play the role of an effective RKKY interaction combined with the appropriate CEF Hamiltonian term (see the Supplemental Material [15]).

Our model does not explicitly include the Kondo interaction but considers it to renormalize the bare spin-spin exchange, so that j_0 and j_1 are effective exchange coupling constants. With this simple mean-field model we calculate the specific heat thermal dependence (see the Supplemental Material [15]) constraining the value of calculated constants to give the zero-field Néel temperature $T_N = 3.8$ K and keeping the experimentally determined ratio $j_0/j_1 \simeq 8$ [36]. For $B = 0$ we find effective $j_0 = 0.72$ K and $j_1 = 0.088$ K, which are an order of magnitude smaller than those derived from a model that gives the zero-field magnetic structure [36]. This is consistent with the fact that thermal fluctuations tend to suppress the mean-field ordering temperature for a quasi-2D system like $CeRhIn_5$ ($j_0/j_1 \simeq 8$).

Following the same approach, we estimate the field dependence of j_0 and j_1, shown in Fig. 2(c), that is required to reproduce the $T_N(B)$ phase boundary [Fig 2(b)]. As seen, j_0 and j_1 decrease linearly up to 30 T before increasing above B^*. From the Shrieffer-Wolff transformation, the Kondo exchange is proportional to the square of the f-c.e. hybridization matrix element [37]. A reasonable interpretation of the increase in exchange constants above B^* then is that this reflects an enhanced hybridization in the high-field state due to field-induced change in the orbital character of the $4f$ wave function. Obviously a more realistic theoretical framework that explicitly takes into account the Kondo interaction as well as a frustrating interlayer next n.n. exchange and orbital degrees of freedom is desirable to substantiate our interpretation.

Our NMR measurements and model calculations thus provide a microscopic basis for the origin of the unusual electronic state that emerges at high fields in the Kondo-lattice $CeRhIn_5$: field-driven mixing of the orbital character of the $4f$ wave function enhances Kondo hybridization that induces a large Fermi surface above $B^* \simeq 30$ T where it experiences a density-wave instability due to nesting at a $\boldsymbol{Q}$ close to, if not the same as, that characterizing magnetic order in the zero-field antiferromagnetic state. There is no detectable change in local structure at fields to 42 T. Except for the field scale B^*, which is specific to the Kondo interaction and crystal-field wave functions of $CeRhIn_5$, similar high-field states should be generic to Kondo-lattice materials. With the essential role of the orbital nature of wave functions and its

consequences for Kondo coupling, B^* could be considered in the zero-temperature limit to reflect an orbitally selective type of Kondo-breakdown quantum-critical point [38,39] within the ordered state. This is an interpretation suggested initially by Jiao *et al.* [1] and now we provide a microscopic rationale for it.

We acknowledge enlightening discussions with F. Ronning, P. F. S. Rosa, M. Smidman, L. Jiao, H. Q. Yuan, D. J. Garcia, C. Rettori, and N. Curro. Work at State University of Campinas (Unicamp) was supported by CNPq (Grants No. 140837/2013-2, No. 307668/2015-0, and No. 309483/2018-2) and FAPESP through Grants No. 2012/05903-6, No. 2012/04870-7, and No. 2017/10581-1 and at Los Alamos by the U.S. Department of Energy, Division of Materials Sciences and Engineering. Part of this work was performed and supported by JSPS KAKENHI through Grant No. JP16KK0106 and by REIMEI Research Program of JAEA. The work at the National High Magnetic Field Laboratory was supported by the National Science Foundation Cooperative Agreement No. DMR-1157490 and the State of Florida.

[1] L. Jiao, Y. Chen, Y. Kohama, D. Graf, E. D. Bauer, J. Singleton, J.-X. Zhu, Z. Weng, G. Pang, T. Shang *et al.*, Proc. Natl. Acad. Sci. U.S.A. **112**, 673 (2015).

[2] P. J. Moll, B. Zeng, L. Balicas, S. Galeski, F. F. Balakirev, E. D. Bauer, and F. Ronning, Nat. Commun. **6**, 6663 (2015).

[3] P. F. S. Rosa, S. M. Thomas, F. F. Balakirev, E. D. Bauer, R. M. Fernandes, J. D. Thompson, F. Ronning, and M. Jaime, Phys. Rev. Lett. **122**, 016402 (2019).

[4] L. Jiao, M. Smidman, Y. Kohama, Z. S. Wang, D. Graf, Z. F. Weng, Y. J. Zhang, A. Matsuo, E. D. Bauer, H. Lee *et al.*, Phys. Rev. B **99**, 045127 (2019).

[5] F. Ronning, T. Helm, K. R. Shirer, M. D. Bachmann, L. Balicas, M. K. Chan, B. J. Ramshaw, R. D. McDonald, F. F. Balakirev, M. Jaime *et al.*, Nature (London) **548**, 313 (2017).

[6] Y. Ando, K. Segawa, S. Komiya, and A. N. Lavrov, Phys. Rev. Lett. **88**, 137005 (2002).

[7] S. A. Kivelson, E. Fradkin, and V. J. Emery, Nature (London) **393**, 550 (1998).

[8] R. M. Fernandes, A. E. Böhmer, C. Meingast, and J. Schmalian, Phys. Rev. Lett. **111**, 137001 (2013).

[9] T.-M. Chuang, M. P. Allan, J. Lee, Y. Xie, N. Ni, S. L. Bud'ko, G. S. Boebinger, P. C. Canfield, and J. C. Davis, Science **327**, 181 (2010).

[10] R. A. Borzi, S. A. Grigera, J. Farrell, R. S. Perry, S. J. S. Lister, S. L. Lee, D. A. Tennant, Y. Maeno, and A. P. Mackenzie, Science **315**, 214 (2007).

[11] D. M. Fobes, S. Zhang, S.-Z. Lin, P. Das, N. J. Ghimire, E. D. Bauer, J. D. Thompson, L. W. Harriger, G. Ehlers, A. Podlesnyak *et al.*, Nat. Phys. **14**, 456 (2018).

[12] N. Aso, K. Ishii, H. Yoshizawa, T. Fujiwara, Y. Uwatoko, G.-F. Chen, N. K. Sato, and K. Miyake, J. Phys. Soc. Jpn. **78**, 073703 (2009).

[13] T. Takeuchi, T. Inoue, K. Sugiyama, D. Aoki, Y. Tokiwa, Y. Haga, K. Kindo, and Y. Onuki, J. Phys. Soc. Jpn. **70**, 877 (2001).

[14] S. Raymond, E. Ressouche, G. Knebel, D. Aoki, and J. Flouquet, J. Phys.: Condens. Matter **19**, 242204 (2007).

[15] See Supplemental Material at http://link.aps.org/supplemental/10.1103/PhysRevB.101.165111 for an introduction to the basics of In-NMR on $CeRhIn_5$; a complementary text and supporting equations for the simulation of the high field spectra; data showing how the single ion Ce magnetization and crystal field orbitals behave as a function of the magnetic field at low temperatures without magnetic ordering; and a calculation of the specific heat based on the mean field model as discussed in the main text.

[16] E. D. Bauer, Y.-f. Yang, C. Capan, R. R. Urbano, C. F. Miclea, H. Sakai, F. Ronning, M. J. Graf, A. V. Balatsky, R. Movshovich *et al.*, Proc. Natl. Acad. Sci. U.S.A. **108**, 6857 (2011).

[17] S. Seo, X. Lu, J.-X. Zhu, R. R. Urbano, N. Curro, E. D. Bauer, V. A. Sidorov, L. D. Pham, T. Park, Z. Fisk *et al.*, Nat. Phys. **10**, 120 (2014).

[18] T. Wu, H. Mayaffre, S. Krämer, M. Horvatić, C. Berthier, W. N. Hardy, R. Liang, D. A. Bonn, and M.-H. Julien, Nature (London) **477**, 191 (2011).

[19] H. Sakai, Y. Tokunaga, S. Kambe, R. R. Urbano, M.-T. Suzuki, P. L. Kuhns, A. P. Reyes, P. H. Tobash, F. Ronning, E. D. Bauer *et al.*, Phys. Rev. Lett. **112**, 236401 (2014).

[20] C. Berthier, M. Horvatić, M.-H. Julien, H. Mayaffre, and S. Krämer, C. R. Phys. **18**, 331 (2017).

[21] Y. Tokunaga, A. Orlova, N. Bruyant, D. Aoki, H. Mayaffre, S. Krämer, M.-H. Julien, C. Berthier, M. Horvatić, N. Higa *et al.*, Phys. Rev. B **99**, 085142 (2019).

[22] N. J. Curro, P. C. Hammel, P. G. Pagliuso, J. L. Sarrao, J. D. Thompson, and Z. Fisk, Phys. Rev. B **62**, R6100 (2000).

[23] N. J. Curro, New J. Phys. **8**, 173 (2006).

[24] S. Kambe, H. Sakai, Y. Tokunaga, R. E. Walstedt, D. Aoki, Y. Homma, and Y. Shiokawa, Phys. Rev. B **76**, 144433 (2007).

[25] T. Ohama, M. Hirano, and S. Noguchi, Phys. Rev. B **71**, 094408 (2005).

[26] Y. Tokunaga, Y. Saito, H. Sakai, S. Kambe, N. Sanada, R. Watanuki, K. Suzuki, Y. Kawasaki, and Y. Kishimoto, Phys. Rev. B **84**, 214403 (2011).

[27] K. R. Shirer, A. C. Shockley, A. P. Dioguardi, J. Crocker, C. H. Lin, N. apRoberts-Warren, D. M. Nisson, P. Klavins, J. C. Cooley, Y.-f. Yang *et al.*, Proc. Natl. Acad. Sci. U.S.A. **109**, E3067 (2012).

[28] Y. Kohori, Y. Yamato, Y. Iwamoto, and T. Kohara, Eur. Phys. J. B **18**, 601 (2000).

[29] C. H. Lin, K. R. Shirer, J. Crocker, A. P. Dioguardi, M. M. Lawson, B. T. Bush, P. Klavins, and N. J. Curro, Phys. Rev. B **92**, 155147 (2015).

[30] N. J. Curro, Rep. Prog. Phys. **79**, 064501 (2016).

[31] Q. Y. Chen, D. F. Xu, X. H. Niu, R. Peng, H. C. Xu, C. H. P. Wen, X. Liu, L. Shu, S. Y. Tan, X. C. Lai *et al.*, Phys. Rev. Lett. **120**, 066403 (2018).

[32] T. Willers, F. Strigari, Z. Hu, V. Sessi, N. B. Brookes, E. D. Bauer, J. L. Sarrao, J. D. Thompson, A. Tanaka, S. Wirth *et al.*, Proc. Natl. Acad. Sci. U.S.A. **112**, 2384 (2015).

[33] A. D. Christianson, J. M. Lawrence, P. G. Pagliuso, N. O. Moreno, J. L. Sarrao, J. D. Thompson, P. S. Riseborough,

S. Kern, E. A. Goremychkin, and A. H. Lacerda, Phys. Rev. B **66**, 193102 (2002).

[34] T. Willers, Z. Hu, N. Hollmann, P. O. Körner, J. Gegner, T. Burnus, H. Fujiwara, A. Tanaka, D. Schmitz, H. H. Hsieh *et al.*, Phys. Rev. B **81**, 195114 (2010).

[35] P. G. Pagliuso, D. J. Garcia, E. Miranda, E. Granado, R. L. Serrano, C. Giles, J. G. S. Duque, R. R. Urbano, C. Rettori, J. D. Thompson *et al.*, J. Appl. Phys. **99**, 08P703 (2006).

[36] P. Das, S.-Z. Lin, N. J. Ghimire, K. Huang, F. Ronning, E. D. Bauer, J. D. Thompson, C. D. Batista, G. Ehlers, and M. Janoschek, Phys. Rev. Lett. **113**, 246403 (2014).

[37] J. R. Schrieffer and P. A. Wolff, Phys. Rev. **149**, 491 (1966).

[38] C. Pépin, Phys. Rev. Lett. **98**, 206401 (2007).

[39] Q. Si, S. Rabello, K. Ingersent, and J. L. Smith, Nature (London) **413**, 804 (2001).